HELDA
HELSINGIN YLIOPISTO
HELSINGFORS UNIVERSITET
UNIVERSITY OF HELSINKI

UNIVERSITY OF HELSINKI

https://helda.helsinki.fi

Density functional theory calculation of the properties of carbon vacancy defects in silicon carbide

Wang, Xiuhong

2020-12

Wang , X , Zhao , J , Xu , Z , Djurabekova , F , Rommel , M , Song , Y & Fang , F 2020 , ' Density functional theory calculation of the properties of carbon vacancy defects in silicon carbide ' , Nami Jishu yu Jingmi Gongcheng = Nanotechnology and Precision Engineering , vol. 3 , no. 4 , pp. 211-217 . https://doi.org/10.1016/j.npe.2020.11.002

http://hdl.handle.net/10138/340689
https://doi.org/10.1016/j.npe.2020.11.002

cc_by_nc_nd
publishedVersion

Downloaded from Helda, University of Helsinki institutional repository.

This is an electronic reprint of the original article.

This reprint may differ from the original in pagination and typographic detail.

Please cite the original version.

Nanotechnology and Precision Engineering

Density functional theory calculation of the properties of carbon vacancy defects in silicon carbide

Cite as: Nanotechnol. Precis. Eng. **3**, 211 (2020); https://doi.org/10.1016/j.npe.2020.11.002
Published Online: 09 March 2021

Xiuhong Wang, Junlei Zhao, Zongwei Xu, et al.

COLLECTIONS

Paper published as part of the special topic on Wide Bandgap (WBG) Semiconductors: from Fundamentals to Applications

EP This paper was selected as an Editor's Pick

View Online Export Citation

ARTICLES YOU MAY BE INTERESTED IN

Confocal photoluminescence characterization of silicon-vacancy color centers in 4H-SiC fabricated by a femtosecond laser
Nanotechnology and Precision Engineering **3**, 218 (2020); https://doi.org/10.1016/j.npe.2020.11.003

Advances in graphene reinforced metal matrix nanocomposites: Mechanisms, processing, modelling, properties and applications
Nanotechnology and Precision Engineering **3**, 189 (2020); https://doi.org/10.1016/j.npe.2020.12.003

Surface defects in 4H-SiC homoepitaxial layers
Nanotechnology and Precision Engineering **3**, 229 (2020); https://doi.org/10.1016/j.npe.2020.12.001

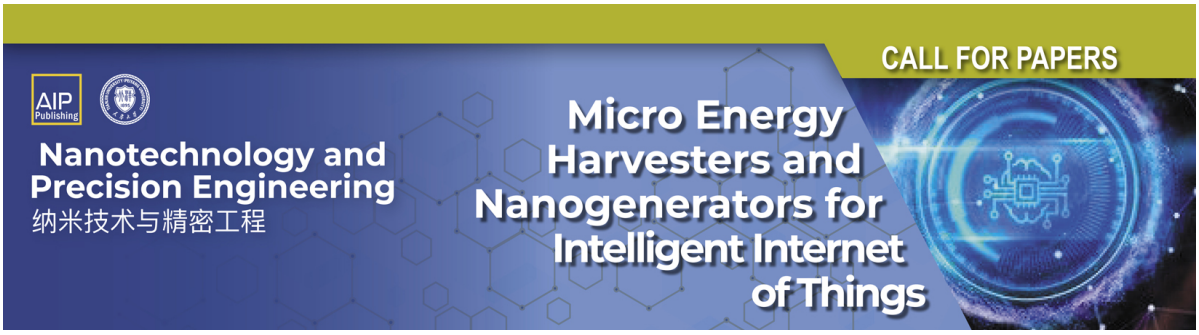

Copyright © 2020 Tianjin University. Publishing Service by Elsevier B.V. on behalf of KeAi Communications Co., Ltd.

Nanotechnology and Precision Engineering 3 (2020) 211–217

Nanotechnology and Precision Engineering

Density functional theory calculation of the properties of carbon vacancy defects in silicon carbide

Xiuhong Wang [a,b], Junlei Zhao [b,c,*], Zongwei Xu [a,**], Flyura Djurabekova [b], Mathias Rommel [d], Ying Song [a], Fengzhou Fang [a]

[a] State Key Laboratory of Precision Measuring Technology & Instruments, Centre of MicroNano Manufacturing Technology, Tianjin University, Tianjin 300072, China
[b] Department of Physics and Helsinki Institute of Physics, University of Helsinki, P.O. Box 43, FI-00014 Helsinki, Finland
[c] Department of Electrical and Electronic Engineering, Southern University of Science and Technology, Shenzhen 518055, China
[d] Fraunhofer Institute for Integrated Systems and Device Technology IISB, Schottkystrasse 10, 91058 Erlangen, Germany

ARTICLE INFO

Available online 11 December 2020

Keywords:
Density functional theory
Silicon carbide
Carbon vacancy

ABSTRACT

As a promising material for quantum technology, silicon carbide (SiC) has attracted great interest in materials science. Carbon vacancy is a dominant defect in 4H-SiC. Thus, understanding the properties of this defect is critical to its application, and the atomic and electronic structures of the defects needs to be identified. In this study, density functional theory was used to characterize the carbon vacancy defects in hexagonal (h) and cubic (k) lattice sites. The zero-phonon line energies, hyperfine tensors, and formation energies of carbon vacancies with different charge states (2^-, $^-$, 0, $^+$ and 2^+) in different supercells (72, 128, 400 and 576 atoms) were calculated using standard Perdew–Burke–Ernzerhof and Heyd–Scuseria–Ernzerhof methods. Results show that the zero-phonon line energies of carbon vacancy defects are much lower than those of divacancy defects, indicating that the former is more likely to reach the excited state than the latter. The hyperfine tensors of $V_C^+(h)$ and $V_C^+(k)$ were calculated. Comparison of the calculated hyperfine tensor with the experimental results indicates the existence of carbon vacancies in SiC lattice. The calculation of formation energy shows that the most stable carbon vacancy defects in the material are $V_C^{2+}(k)$, $V_C^+(k)$, $V_C(k)$, $V_C^-(k)$ and $V_C^{2-}(k)$ as the electronic chemical potential increases.
Copyright © 2020 Tianjin University. Publishing Service by Elsevier B.V. on behalf of KeAi Communications Co., Ltd. This is an open access article under the CC BY-NC-ND license (http://creativecommons.org/licenses/by-nc-nd/4.0/).

1. Introduction

As a wide band gap semiconductor, silicon carbide (SiC) plays an important role in the power electronics industry owing to its advantages of high electronic breakdown field, high thermal conductivity, and chemical stability.[1–3] SiC has different polytypes, of which 3C, 4H, and 6H are the most common ones. Moreover, 4H-SiC is suitable for manufacturing high-power electronic devices because of its large forbidden band width (3.26 eV), good thermal conductivity, and relatively small anisotropy.[4–6]

So far, research on the growth of 4H-SiC has made remarkable achievements.[7–9] Carbon vacancy (V_C) is a significant defect with strong and harmful effects on the carrier lifetime of 4H-SiC.[10,11] Previous studies used electron paramagnetic resonance to show V_C^+ defects in P-type 4H-SiC annealed at high temperatures and analyzed the influence of external environmental changes on the defects, but some basic electrical properties of V_C^+ defects remain to be characterized.[12] Point defects in SiC were theoretically studied employing pseudopotential calculations without full ionic relaxations and using only a small supercell.[13] Recent studies have performed accurate pseudopotential calculations with full ionic relaxations employing a large supercell.[14–17] Nevertheless, the present understanding of point defects in SiC remains incomplete.

Therefore, the present study used the first-principles method to characterize the geometric structure and electrical properties of the carbon vacancy in 4H-SiC supercell. The defects at cubic and hexagonal lattice sites were considered separately in our calculations.

The outline of the article is as follows. Section 2 describes the calculation details and model. Section 3 presents the results for the carbon vacancy defects: zero-phonon line energy, hyperfine tensor, and formation energy curves. Finally, Section 4 discusses the results of the properties of carbon vacancy defects in SiC.

2. Calculation details and model

2.1. Details of calculation

Density functional theory (DFT) calculations were carried out using the 5.4.4 version of Vienna Ab Initio Simulation Package (VASP).[18,19]

* Corresponding author at: Department of Physics and Helsinki Institute of Physics, University of Helsinki, P.O. Box 43, FI-00014 Helsinki, Finland.
** Corresponding author at: State Key Laboratory of Precision Measuring Technology & Instruments, Centre of MicroNano Manufacturing Technology, Tianjin University, Tianjin 300072, China.
E-mail addresses: zhaojl@sustech.edu.cn (J. Zhao), zongweixu@tju.edu.cn (Z. Xu).

https://doi.org/10.1016/j.npe.2020.11.002
2589-5540/Copyright © 2020 Tianjin University. Publishing Service by Elsevier B.V. on behalf of KeAi Communications Co., Ltd. This is an open access article under the CC BY-NC-ND license (http://creativecommons.org/licenses/by-nc-nd/4.0/).

The projector augmented wave (PAW) method was employed to describe the core electrons.[18,20,21] Spin-polarized electronic structure calculations were carried out using the Perdew–Burke–Ernzerhof (PBE)[22] and Heyd–Scuseria–Ernzerh of (HSE06)[23] exchange-correlation functionals. For SiC, the HSE06 functional provides accurate results while considering the contribution of the spin polarization of the core electrons to the Fermi-contact term.[23]

Plane-wave basis with kinetic energy up to 420 eV was used to describe the Kohn–Sham electronic states. For defect modeling, the unit cell must be optimized. The optimized lattice constants and band gaps for the 4H–SiC unit cell were obtained using a Monkhorst–Pack grid of $9 \times 9 \times 5$ with a plane-wave cut-off energy of 420 eV.[24] In this calculation, the electronic and ionic convergence thresholds were set as 1×10^{-5} eV and 1×10^{-4} eV, respectively.

2.2. Model

The basic structural unit of 4H-SiC is Si—C tetrahedron, wurtzite structure and belongs to the hexagonal crystal system. Its stacking method is ABCB type. The theoretical model of 4H-SiC is shown in Fig. 1. The large atoms in the figure are silicon, and the small atoms are carbon. The crystal of this structure is an AB-type covalent bond crystal, and each silicon atom is surrounded by four carbon atoms bonded by oriented strong tetrahedral sp3 bonds. Each 4H-SiC unit cell contains four silicon atoms and four carbon atoms. The space group of 4H-SiC is P6_3 mc, and the lattice constants are $a = b =$ 3.073 Å and $c =$ 10.053 Å. For defect modeling, large 72, 128, 400, and 576 atom supercells were applied for 4H-SiC. Fig. 2 shows the structure of a carbon vacancy defect containing 576 atomic supercells.

3. Results and discussion

The basic structure and energy band of the 4H-SiC unit cell were calculated to ensure the accuracy of the 4H-SiC model. Only under the premise of obtaining sufficiently good results can the electrical properties of the 4H-SiC supercell structure containing carbon vacancy defects be calculated.

3.1. 4H-SiCunit cell calculation results

3.1.1. Structure of crystal lattice

The structure, including the atomic position and lattice parameters, of the 4H-SiC unit cell is optimized using the PBE exchange-correlation functional. Fig. 3 shows the optimization results of the lattice constants of the 4H-SiC unit cell structure. Fig. 3(a) is the optimization

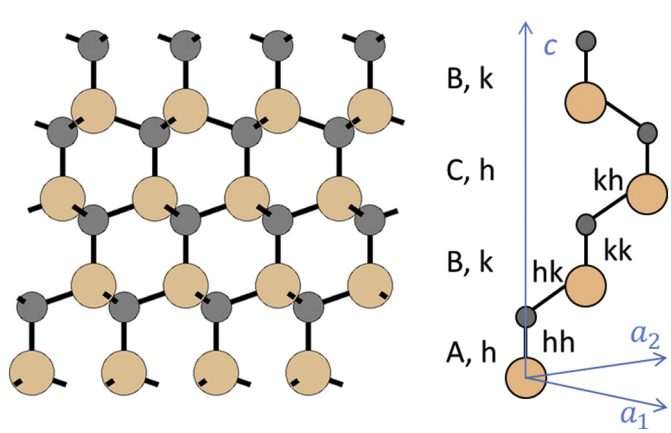

Fig. 1. The structure of 4H–SiC. Upper-case letters show the stacking of Si—C double layers, and lower-case letters show whether or not the double layers and their immediate surroundings follow a cubic-like (k) or a hexagonal-like (h) stacking order.

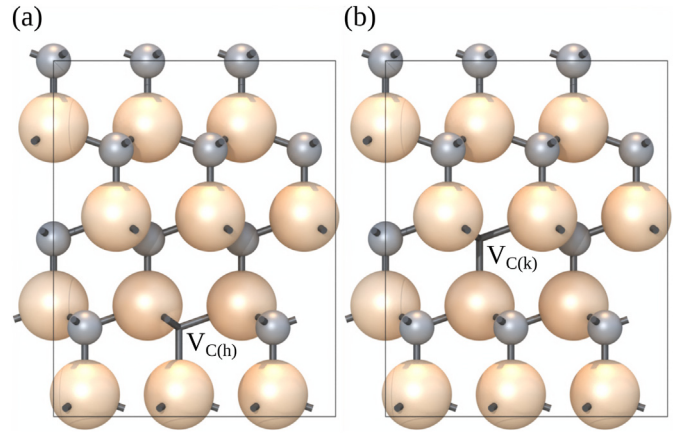

Fig. 2. Carbon vacancy defect structure. (a) Hexagonal carbon vacancy defect; (b) Cubic carbon vacancy defect.

of lattice constants a and b, and Fig. 3(b) is the optimization of lattice constant c. Finally, the lattice constants of the 4H-SiC unit cell are $a = b =$ 3.094 Å and $c =$ 10.125 Å. The results are the same as those calculated by Davidsson et al.[25] Compared with the experimental value, calculated lattice constants differ by about 0.7%, which agrees well with the experimental value. This result indicates that the PAW pseudopotential and PBE exchange-correlation functional used in the simulation calculation can describe the structure of the 4H-SiC well.

3.1.2. Energy band structures

On the basis of the previously optimized 4H-SiC unit cell structure, the electrical properties of the 4H-SiC unit cell can be calculated non-self-consistently. The choice of exchange-correlation functional in the calculation may lead to a large difference in the energy band calculation results. Two exchange-correlation functionals (PBE and HSE06) are used in the calculation of the 4H-SiC unit cell to obtain accurate calculation results. The energy band results under different exchange-correlation functionals were compared, and the result closer to the true value was selected for the subsequent non-self-consistent calculation of the supercell.

Given that 4H-SiC has a hexagonal crystal structure, the high symmetric K-point path of the Brillouin zone used in the calculation is $\Gamma \rightarrow M \rightarrow K \rightarrow \Gamma \rightarrow A \rightarrow L \rightarrow H \rightarrow A$, where the Γ point is Brillouin in the center of the district. The path of high-symmetry points is shown in Fig. 4, and the K point used is $9 \times 9 \times 5$. Fig. 5 shows the calculation results of the two exchange-correlation functionals.

Fig. 5(a) shows the energy band structure calculated using the PBE exchange-correlation functional method. The 4H-SiC band gap width is 2.63 eV, which is different from the experimental result of 3.26 eV but is similar to the calculated result of Cheng et al.[26] This discrepancy can be ascribed to the fact that the PBE functional underestimates the correlation between excited state electrons, which explains the low calculation result of the energy band. The energy band result using the HSE06 functional obtained is shown in Fig. 5(b). In addition, the band gap of the 4H-SiC unit cell is 3.18 eV, which is close to the experimental result of 3.26 eV with a difference of about 2.4%. The result is similar to the 3.19 eV calculated by Yan et al.[27] The valence band maximum of the 4H-SiC energy band diagram is at Γ point, and the conduction band minimum (CBM) is at M point, which is an indirect band gap semiconductor. The comparison shows that the HSE06 functional is more accurate than the PBE functional in describing the energy band structure of 4H-SiC.

3.2. Electrical properties of carbon vacancy defects in 4H-SiC supercells

On the basis of the previously optimized unit cell structure, 4 supercell models of $3 \times 3 \times 1$, $4 \times 4 \times 1$, $5 \times 5 \times 2$ and $6 \times 6 \times 2$ were

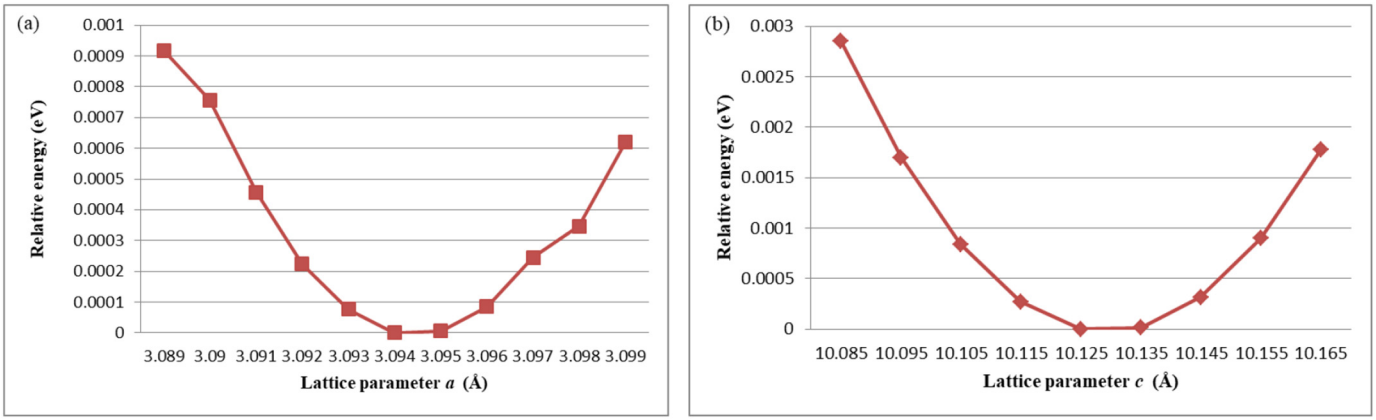

Fig. 3. Lattice optimization results of the 4H-SiC unit cell structure. (a) Lattice constant *a*; (b) Lattice constant *c*.

established, respectively, that is, the supercells contain 72, 128, 400 and 576 atoms, respectively. In actual calculations, the calculation cost of the HSE06 functional is excessively large, and the calculation time is excessively long. Therefore, the PBE functional was used to simulate the supercell structure. It has little effect on comparing the results of different super cells. The lattice constant, Fermi level, zero-phonon line energy, formation energy, and hyperfine tensor of the carbon vacancy defects were calculated, and the structural and electrical properties of the carbon vacancy defects at two different lattice positions were systematically studied.

3.2.1. Lattice constant

The supercell structure needs to be optimized. Table 1 shows the corresponding lattice structure parameters of each supercell.

For the same supercell, the lattice constant of the supercell containing carbon vacancy defects is smaller than that of the supercell without defects. This result can be ascribed to the fact that the supercell containing carbon vacancy defects loses a carbon atom compared with the perfect supercell. As a result, the force between atoms adjacent to the carbon atom weakens, and the lattice constant becomes smaller. The carbon vacancy defects at two different lattice positions have almost the same effect on the lattice constant of the material because they both lose a carbon atom, and the interaction forces of carbon atoms at different lattice positions are almost the same. As the supercell increases (72 atoms to 576 atoms), the lattice constant *a* of the defect gradually increases, and the lattice constant *c* gradually decreases because the defect concentration decreases with the increase in supercells.

3.2.2. Fermi level

The charged defects may have a certain impact on the Fermi level. Thus, the Fermi level of the carbon vacancy defects with a positive charge on the two lattice positions was calculated. A static self-consistent calculation was performed on the basis of the optimized supercell to obtain its Fermi level, as shown in Table 2.

For the same supercell, the Fermi levels of $V_C(h)$, $V_C(k)$, $V_C^+(h)$, and $V_C^+(k)$ all move to a higher energy because the supercell with defects is smaller than the perfect supercell, and the number of electrons carried by carbon atoms is less than the number of electrons carried by silicon atoms. Thus, the number of valence electrons per unit volume is increased, andthe Fermi level of the supercell with defects increases.

3.2.3. Zero-phonon line energy

The zero-phonon line energy is the difference between the energy of the ground state and the energy of the excited state. Therefore, understanding the ground-state and excited-state electronic structures of the carbon vacancy defects is necessary, as shown in Fig. 6. In this section, the zero-phonon line energy of the double-vacancy defect was also calculated to understand the carbon vacancy defect. The calculation result is shown in Fig. 7.

Fig. 7 shows a comparison of the zero-phonon line energy of the defects under different supercells. Results show that the zero-phonon line of the defect gradually converges as the supercell increases. In the case of a supercell with 72 atoms, the defect concentration is large, which makes the results unreliable. When the supercell contains 576 atoms, the zero-phonon line energy of the double-vacancy defect is 1.046 eV, which is similar to the calculation results of others.[25,28] The zero-phonon line energy of the $V_C(h)$ defect is 0.216 eV, and the zero-phonon line energy of the $V_C(k)$ defect is 0.414 eV. As seen in Fig. 7, the calculated values of ZPL energy using $4 \times 4 \times 1$ supercell (128 atoms) are very close to those calculated values which use $5 \times 5 \times 2$ and $6 \times 6 \times 2$ supercells, therefore, $4 \times 4 \times 1$ supercell is large enough for the calculations of ZPL energy of carbon vacancy and double vacancy. The zero-phonon line energy of the carbon vacancy defects is much lower than that of the double-vacancy defects. This result indicates that the single-vacancy defects more easily reach the excited state than the double-vacancy defects.

3.2.4. Formation energy

Defect formation energy is an important concept that directly reflects the difficulty of formation of defects and the degree of stability of defects in the material. It can also reflect the concentration of defects in the material to a certain extent. Therefore, calculating defect formation energy is important for the study of carbon vacancy defects in 4H-SiC. This section mainly studies the formation energies of carbon vacancy defects with different charges based on the structure of these two lattice positions. The formation energy of charged defects in this article is calculated as follows[29]:

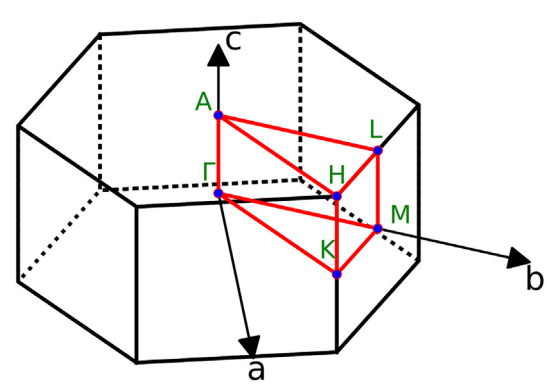

Fig. 4. Path of high-symmetry points.

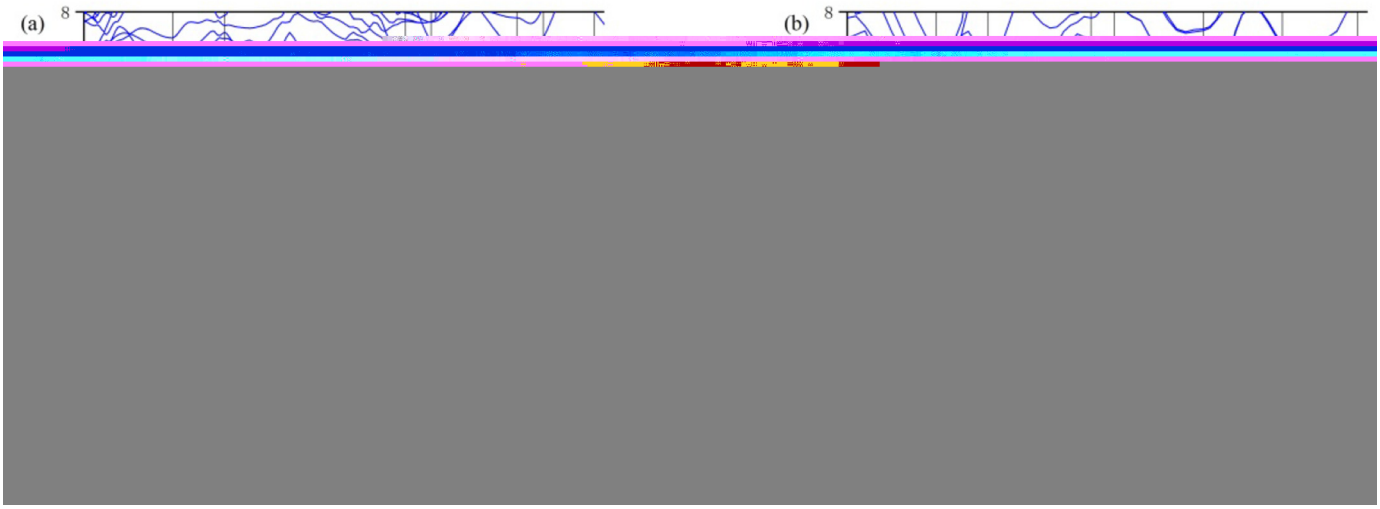

Fig. 5. 4H-SiC energy bands calculated by (a) the PBE functional and (b) the HSE06 functional.

Table 1
Lattice parameters of perfect unit cells of different sizes of supercells and supercells containing carbon vacancy defects.

Atoms	72		128		400		576	
Lattice constants	*a* (Å)	*c* (Å)	*a* (Å)	*c* (Å)	*a* (Å)	*c* (Å)	*a* (Å)	*c* (Å)
Supercell	3.094	10.125	3.094	10.125	3.094	10.125	3.094	10.125
V_C(h)	3.086	10.139	3.088	10.129	3.089	10.120	3.090	10.119
V_C(k)	3.087	10.126	3.088	10.126	3.089	10.120	3.090	10.119

Table 2
Relative Fermi levels (eV) of perfect unit cells of different sizes of supercells and supercells with defects.

Atoms	72	128	400	576
Supercell	0	0	0	0
V_C(h)	1.415	1.401	1.509	1.530
V_C(k)	1.399	1.384	1.414	1.431
V_C^+(h)	0.878	0.921	0.879	0.832
V_C^+(k)	0.957	0.941	0.875	0.919

$$E_f(q) = E_{def}(q) - E_0 - \sum_i u_i n_i + q(E_{VBM} + E_F) + E_{FNV}{}^q \quad (1)$$

where $E_{def}(q)$ represents the total energy of supercells containing carbon vacancy defects, E_0 represents the total energy of supercells without defects, n_i represents the number of atoms added or removed in the supercell (for carbon vacancy defects, it means losing an atom), u_i represents the chemical potential of adding or removing atoms, that is, the chemical potential of carbon atoms, E_{VBM} represents the VBM corresponding to the supercell containing the defect, and E_F represents the energy corresponding to the Fermi level (i.e., the electronic chemical potential), and it varies from zero to the forbidden band width.

However, when calculating the defect formation energy, false interactions of charged defects occur because the periodic boundary conditions are used to construct the supercell model. Such interactions affect the total energy of the supercell. For such a situation, the Freysoldt, Neugebauer, and Van de Walle (FNV) scheme is used to make corrections to obtain realistic results.[29] The key idea of the FNV scheme is to introduce the real charge distribution to simulate the actual distribution of the charge carried by the defect.

A supercell with 128 atoms is used to calculate the formation energy of defects with different charges and lattice positions in 4H-SiC. The calculation parameters are the same as the previous calculations. The calculation results are shown in Fig. 8.

The left image in Figure8shows the variation in the formation energy corresponding to the 10 types of carbon vacancy defects with the electronic chemical potential, and the right image is an enlarged view of the box in the left image. Calculation results show that the formation energy of V_C(k) defects in 4H-SiC is 4.857 eV, and the formation energy of V_C(h) defects is 4.917 eV. The results are similar to those calculated by Kobayashi et al.[30] The formation energy does not change with the change in electronic chemical potential. That is, the formation energy of neutral charge-state defects remains unchanged regardless of whether the 4H-SiC material is N-type or P-type. The charged defects change with the crystal environment and with the increase in the

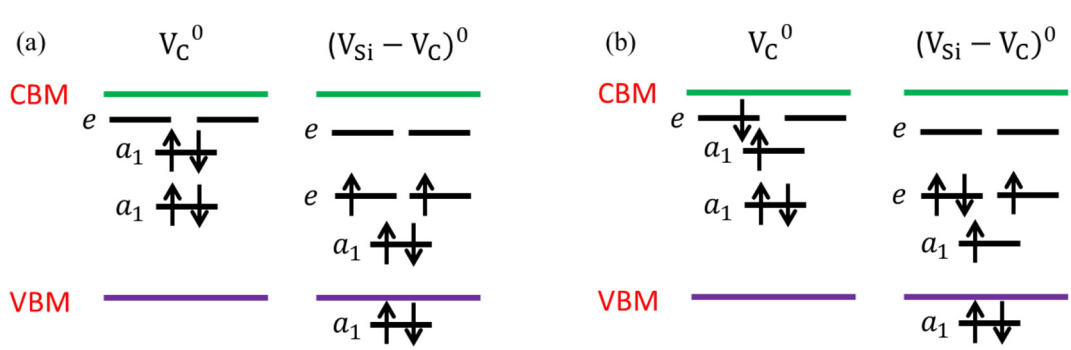

Fig. 6. Ground-state and excited-state electronic structures of the carbon vacancy and double-vacancy defects. (a) Ground-state electronic structure; (b) Excited-state electronic structure.

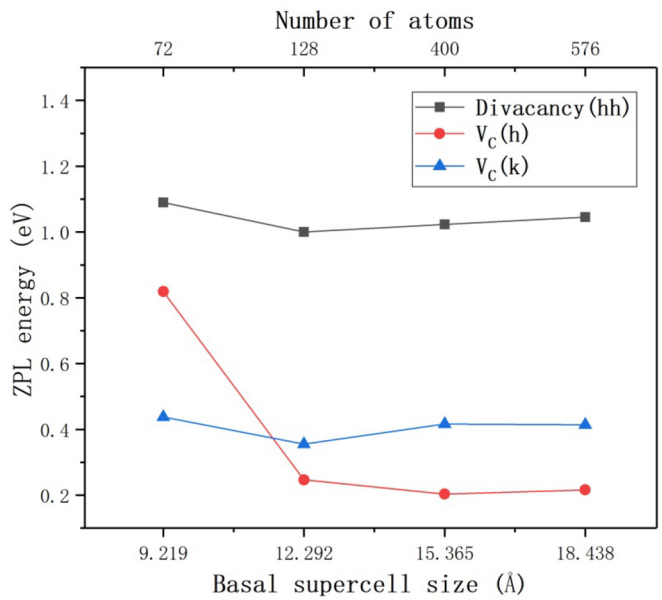

Fig. 7. Zero-phonon line (ZPL) energy of carbon vacancy and double-vacancy defects under different supercells.

electronic chemical potential. In the transition of 4H-SiC from P-type to high purity to N-type, the most stable defects in 4H-SiC are V_C^{2+}(k), V_C^{+}(k), V_C(k), V_C^{-}(k), and V_C^{2-}(k). Cheng et al.[31] also showed that the concentration of carbon vacancy defects is the highest in 4H-SiC. In P-type 4H-SiC, the formation energy of positively charged carbon vacancy defects is the lowest, indicating that most of the carbon vacancy defects are positively charged. In N-type 4H-SiC, the formation energy of negatively charged carbon vacancy defects is the lowest. This result shows that most of the carbon vacancy defects are negatively charged, whereas the defects in high-purity silicon carbide (SiC) are generally not charged. Among the carbon vacancies of the same charge, the formation energy of the carbon vacancy defects in the hexagonal lattice position is always greater than that in the cubic lattice position. This result indicates that the carbon vacancy defects in the cubic lattice position form more easily and have a higher concentration than those in the hexagonal lattice position. It is consistent with the conclusion of Capan et al.[32]

3.2.5. Hyperfine tensor

Hyperfine coupling (also called hyperfine interaction) refers to the interaction between unpaired electron spin and nuclear spin. If magnetic nuclei exist around the unpaired electrons, a single EPR line will split into many narrower lines under the hyperfine interaction. These lines are the hyperfine structure of the spectrum. In the previous work,[12] the hyperfine tensors of the two types of carbon vacancy defects were obtained by electron paramagnetic resonance. In this section, the hyperfine tensors for these two types of carbon vacancy defects were calculated. The results are shown in Table 3 and Table 4. These tables only record the hyperfine tensor value of the carbon vacancy defects and the four nearest silicon atoms, which is sufficient for identifying the defect structure. Among them, *x*, *y* and *z* are the hyperfine tensor values in three directions, and the bolded parts in these tables are the results of Ref. [33]. The supercell selected in Ref. [33] contains 128 atoms.

As listed in Table 3, for the carbon vacancy at the hexagonal lattice position V_C^{+}(h), the hyperfine tensor results converge gradually with the increase in supercell and are close to the experimental results in the previous work.[12] The interaction between the nucleus and the electron cloud can be well described by using the PAW method and the PBE functional. In addition, V_C^{+}(h) has C_{3v} symmetry. Table 3 shows that the hyperfine tensor results corresponding to the supercell with only 72 atoms have a large deviation compared to results for larger cells because the supercell of 72 atoms is too small, which leads to the high concentration of defects in the material. As a result, the hyperfine tensor results are not accurate. However, Table 4 displays that for the carbon vacancy in the cubic lattice V_C^{+}(k), the exchange-correlation functional PBE may not describe the hyperfine tensors of carbon vacancy defects in SiC. In addition, the pseudopotential in the VASP software selected in this article is not the same as the references. With the increase of supercell atoms, the hyperfine tensors of V_C^{+}(h) defects tend to be V_C^{+}(k) defects, and the hyperfine tensor values of V_C^{+}(k) defects in the VASP system do not reach a steady state, leading to the transformation of defects.

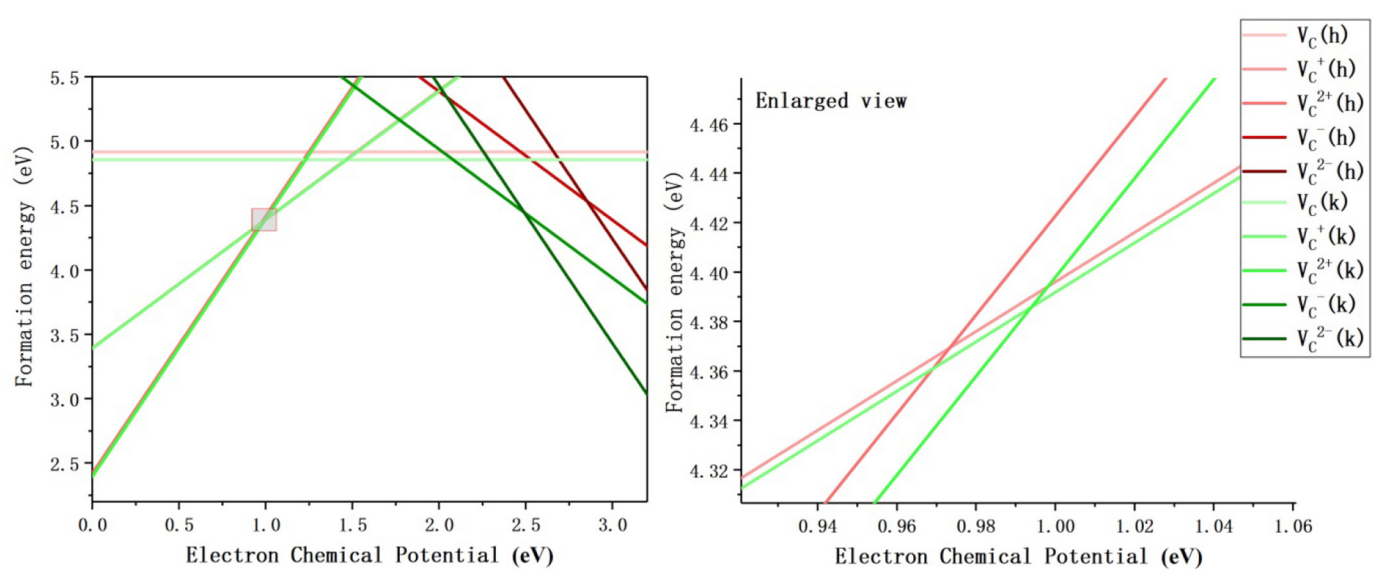

Fig. 8. Calculation results of the formation energy of carbon vacancy defects with different charges and lattice positions.

Table 3
Hyperfine tensor calculation results of $V_C^+(h)$ defects.

$V_C^+(h)$	Atoms	Hyperfine tensor (MHz)		
		x	*y*	*z*
$A(Si_1)$	72	199.9	199.9	290.0
	128	313.9	313.9	461.0
	400	307.9	308.0	455.1
	576	307.2	307.2	454.5
	Ref[33]	**275**	**275**	**400**
$A(Si_{2-4})$	72	125.1	124.3	156.1
	128	21.8	19.9	36.2
	400	21.0	18.9	35.5
	576	21.1	19.1	35.34
	Ref[33]	**22**	**20**	**43**

Table 4
Hyperfine tensor calculation results of $V_C^+(k)$ defects.

$V_C^+(k)$	Atoms	Hyperfine tensor (MHz)		
		x	*y*	*z*
$A(Si_1)$	72	154.2	154.2	207.8
	128	292.3	292.3	409.0
	400	336.5	336.5	476.9
	576	341.5	341.5	484.9
	Ref.[33]	**122**	**114**	**197**
$A(Si_{2-4})$	72	157.5	157.4	200.3
	128	68.7	68.0	88.3
	400	35.8	33.6	48.6
	576	33.2	30.7	45.4
	Ref.[33]	**93**	**78**	**155**

4. Conclusions

The energy levels and electrical properties of carbon vacancy defects in 4H-SiC were calculated by first-principles VASP software. Aiming at the carbon vacancy defects in SiC, this study investigated the effect of defect concentration on the experiment by changing the size of the supercell. This article plays a guiding role in the preparation of high-purity SiC materials. Given the existence of two lattice positions in 4H-SiC, two types of carbon vacancy defects appear in different lattice positions: $V_C^+(h)$ and $V_C^+(k)$. Considering the influence of defect concentration on the calculation results, the lattice constants and Fermi levels of supercells with different sizes (72, 128, 400 and 576 atoms) are calculated. The results show that the lattice constants of supercells with carbon vacancy defects are smaller than those of perfect supercells because supercells with defects lose a carbon atom relative to the perfect supercells, which weakens the interaction force between the atoms adjacent to the carbon atom, thus decreasing the lattice constant. For the Fermi level, with the increase in the number of atoms in the supercell, the Fermi level of the perfect lattice moves to the lower energy band. For the same supercell, the Fermi levels of $V_C(h)$, $V_C(k)$, $V_C^+(h)$, and $V_C^+(k)$ all move to the higher energy.Then, the zero-phonon lines of two kinds of defect structures were calculated. The results show that for the two-carbon vacancy defects, their zero-phonon line energy is considerably far lower than the double-vacancy zero-phonon line energy, that is, the carbon vacancy defects more easily reach the excited state than the double-vacancy defects. Then, the formation energies of 10 types of defect structures in 4H-SiC were calculated. The formation energy of $V_C(k)$ defects in 4H-SiC is 4.857 eV, and the formation energy of $V_C(h)$ defects is 4.917 eV. The results also show that with the increase in the electronic chemical potential, the most stable defect in 4H-SiC is $V_C^{2+}(k)$, $V_C^+(k)$, $V_C(k)$, $V_C^-(k)$ and $V_C^{2-}(k)$. In the same charge state, the formation energy of carbon vacancy defects in the hexagonal lattice is always greater than that in the cubic lattice, which indicates that the carbon vacancy defects in the cubic lattice form more easily and have higher concentration than those in the hexagonal lattice.

Declaration of Competing Interest

None.

Acknowledgments

The study is supported by the National Natural Science Foundation of China (No. 51575389, 51761135106), the National Key Research and Development Program of China (No. 2016YFB1102203), the State Key Laboratory of Precision Measuring Technology and Instruments (Pilt1705), and the “111” Project by the State Administration of Foreign Experts Affairs and the Ministry of Education of China (No. B07014). Computational research performed at the University of Helsinki was supported by the EU Project M4F (Project ID: 755039). CSC-IT Center for Science, Finland, is acknowledged for providing the computational resources. The authors thank Dr. Ilja Makkonen and Dr. Joel Davidsson for the helpful discussion. The authors also thank for the valuable discussions with Mr. Fei Ren from Lanzhou University and Prof. Dejun Wang from Dalian University of Technology.

References

1. Weitzel CE, Palmour JW, Carter CH, et al. Silicon carbide high-power devices. IEEE Trans Electron Dev 1996;43(10):1732-41.
2. Roccaforte F, Fiorenza P, Greco G, et al. Emerging trends in wide band gap semiconductors (SiC and GaN) technology for power devices. Microelectron Eng 2018(187–188):66-77https://doi.org/10.1016/j.mee.2017.11.021.
3. Wei R, Song S, Yang K, et al. Thermal conductivity of 4H-SiC single crystals. J Appl Phys 2013;113(5), 053503https://doi.org/10.1063/1.4790134.
4. Wenzien B, Käckell P, Bechstedt F. Quasiparticle band structure of silicon carbide polytypes. Phys Rev B 1995;52(15):10897-905https://doi.org/10.1103/PhysRevB.52.10897.
5. Roccaforte F, Fiorenza P, Greco G, et al. Challenges for energy efficient wide band gap semiconductor power devices. Physica Status Solidi (A) Appl Mater Sci 2014;211(9):2063-71https://doi.org/10.1002/pssa.201300558.
6. Izhevskyi VA, Genova LA, Bressiani JC, et al. Silicon carbide. Structure, properties and processing. Cerâmica 2000;46(297):4-13https://doi.org/10.1590/S0366-69132000000100002.
7. Hsiao TC, Tsao S. Synthesis and purification of silicon carbide powders for crystal growth. Mater Sci Forum 2012(717–720):37-40.
8. Kojima K, Okumura H, Kuroda S, et al. Homoepitaxial growth of 4H-SiC on on-axis (0001) C-face substrates by chemical vapor deposition. J Cryst Growth 2004;269(2–4):367-76.
9. Itoh A, Kimoto T, Matsunami H. Exciton-related photoluminescence in 4H-SiC growm by step-controlled epitaxy. Jpn J Appl Phys 1996;35(8):4373-8.
10. Gali A, Son NT, Janzén E. Electrical characterization of metastable carbon clusters in SiC: a theoretical study. Phys Rev B 2006;73(3):3204https://doi.org/10.1103/PhysRevB.73.033204.
11. Zvanut ME, Lee WW, Wang HY, et al. Deep level point defects in semi-insulating SiC. Mater Sci Forum 2006(527–529):517-22. 10.4028/www.scientific.net/MSF.527-529.517.
12. Wang X, Xu Z, Rommel M, et al. Electron paramagnetic resonance characterization of aluminum ion implantation-induced defects in 4H-SiC. Nanotechnol Precision Engi 2019;2(4):157-62.
13. Wang C, Bernholc J, Davis R. Formation energies, abundances, and the electronic structure of native defects in cubic SiC. Physical Rev B Condens Matter 1988;38(17):12752-5https://doi.org/10.1103/PhysRevB.38.12752.
14. Zywietz A, Furthmüller J, Bechstedt F. Spin state of vacancies: from magnetic Jahn-teller distortions to multiplets. Phys Rev B 2000;62(11):6854-7.
15. Puska MJ, Pöykkö S, Pesola M, et al. Convergence of supercell calculations for point defects in semiconductors: vacancy in silicon. Phys Rev B 1998;58(3):1318-25https://doi.org/10.1103/PhysRevB.58.1318.
16. Torpo L, Nieminen RM, Laasonen KE, et al. Silicon vacancy in SiC: a high-spin state defect. Appl Phys Lett 1999;74(2):221-3https://doi.org/10.1016/j.physb.2009.09.023.
17. Torpo L, Nieminen RM. Electronic structure of the anti-structure pair in 3C–SiC. Mater Sci Eng B 1999;61–62:593-6https://doi.org/10.1016/S0921-5107(98)00481-4.
18. Kresse G, Furthmüller J. Efficient iterative schemes for ab initio total-energy calculations using a plane-wave basis set. Physical Rev B Condens Matter 1996;54(16):11169-86https://doi.org/10.1103/PhysRevB.54.11169.
19. Kresse G, Joubert D. From ultrasoft pseudopotentials to the projector augmented-wave method. Phys Rev B 1999;59(3):1758-75https://doi.org/10.1103/PhysRevB.59.1758.

20. Yan X, Li P, Kang L, et al. First-principles study of electronic and diffusion properties of intrinsic defects in 4H-SiC. J Appl Phys 2020;127(8), 085702https://doi.org/10.1063/1.5140692.
21. Blöchl PE. Projector augmented-wave method. Phys Rev B 1994;50:17953-79https://doi.org/10.1103/PhysRevB.50.17953.
22. Perdew JP, Burke K, Ernzerhof M. Generalized gradient approximation made simple. Phys Rev Lett 1997;77(18):3865-8.
23. Heyd J, Scuseria GE. Ernzerhof *M. erratum*: "Hybrid functionals based on a screened Coulomb potential" [J. Chem. Phys. 118, 8207 (2003)]. J Chem Phys 2006;124: 219906https://doi.org/10.1063/1.2204597.
24. Monkhorst HJ, Pack JD. Special points for Brillouin-zone integrations. Physical Rev B Condens Matter 1976;16(12):1748-9.
25. Davidsson J, Ivády V, Armiento R, et al. First principles predictions of magneto-optical data for semiconductor defects: the case of divacancy defects in 4H-SiC. New J Phys 2018;20(2), 023035.
26. Cheng P, Zhang YM, Zhang YM, et al. Stability of the intrinsic defects in unintentionally doped 4H-SiC epitaxial layer. Acta Phys Sin 2010;59(5):3542-6.
27. Yan X, Li P, Kang L, et al. First-principles study of electronic and diffusion properties of intrinsic defects in 4H-SiC. J Appl Phys 2020;127(8), 085702https://doi.org/10.1063/1.5140692.
28. Gordon L, Janotti A, Van de Walle CG. Defects as qubits in 3C and 4H-SiC. Phys Rev B 2015;92, 045208.
29. Freysoldt C, Neugebauer J, Walle CGVD. Electrostatic interactions between charged defects in supercells. Phys Status Solidi 2011;248(5):1067-76.
30. Kobayashi T, Harada K, Kumagai Y, et al. Native point defects and carbon clusters in 4H-SiC: a hybrid functional study. J Appl Phys 2019;125(12):125701https://doi.org/10.1063/1.5089174.
31. Cheng P, Zhang YM, Zhang YM. First-principles calculation on the concentration of intrinsic defects in 4H-SiC. J Semicond 2013;1:16-9https://doi.org/10.1088/1674-4926/34/1/013002.
32. Capan I, Brodar T, Pastuovi E, et al. Double negatively charged carbon vacancy at the h- and k-sites in 4H-SiC: combined Laplace-DLTS and DFT study. J Appl Phys 2018;123(16):161597.
33. Bockstedte M, Heid M, Pankratov O. Signature of intrinsic defects in SiC: Ab initio calculations of hyperfine tensors. Phys Rev B 2003;67(19):193102.

Xiuhong Wang, State Key Laboratory of Precision Measuring Technology and Instruments, School of Precision Instruments and Optoelectronics Engineering, Tianjin University. Ms. Wang is studying for Master degree. Her research interests include silicon carbide material and deep level defect.

Junlei Zhao, PhD, Department of Physics, University of Helsinki; Department of Electrical and Electronic Engineering, Southern University of Science and Technology. His research interests include: multi-scale computational modeling of nanomaterials, wide band-gap semiconductor and high-entropy alloy, etc.

Zongwei Xu, Associate Professor, State Key Laboratory of Precision Measuring Technology and Instruments, School of Precision Instrument and Opto-Electronics Engineering, Tianjin University. His research interests include: defect engineering in wide band gap semiconductor, micro/nanofabrication using focused ion beam, Raman and fluorescence spectrum, etc.

Flyura Djurabekova, Professor in Materials in Extreme Environments, Department of Physics, University of Helsinki. Her group studies the materials for accelerator technology within the Accelerator Technology project at HIP by means of different computational methods.

Mathias Rommel, Friedrich-Alexander-Universität Erlangen-Nürnberg (FAU) and Fraunhofer Institute for Integrated Systems and Device Technology IISB, Germany. His research interests include: focused ion beam (FIB), nanoimprint lithography, electrical scanning probe microscopy, and deep level transient spectroscopy (DLTS).

Ying Song is working in the area of manufacturing and spectral characterization of silicon carbide color centers, including the preparation of silicon carbide color centers by ion-implantation, three-dimensional Raman and photoluminescence spectral characterization, and model of spectral depth profiling.

Fengzhou Fang, Professor, State Key Laboratory of Precision Measuring Technology and Instruments, School of Precision Instrument and Opto-Electronics Engineering, Tianjin University. His research interests are in the areas of micro/nano manufacturing, optical freeform manufacturing, bio-medical manufacturing, and ultra-precision machining and metrology.